Available online at www.sciencedirect.com
ScienceDirect
Acta Materialia xxx (2009) xxx–xxx
Acta MATERIALIA
www.elsevier.com/locate/actamat

Application of ultrasonic methods to determine elastic anisotropy of polycrystalline copper processed by equal-channel angular pressing

Hanuš Seiner [a,b,*], Lucie Bodnárová [a,b], Petr Sedlák [a,b], Miloš Janeček [c], Ondřej Srba [c], Robert Král [c], Michal Landa [a]

[a] Institute of Thermomechanics, Academy of Sciences of the Czech Republic, Dolejškova 5, 18200 Prague, Czech Republic
[b] Faculty of Nuclear Sciences and Physical Engineering, Czech Technical University in Prague, Trojanova 13, 12000 Prague, Czech Republic
[c] Faculty of Mathematics and Physics, Charles University, Ke Karlovu 5, 12116 Prague, Czech Republic

Received 27 May 2009; received in revised form 31 August 2009; accepted 31 August 2009

Abstract

Anisotropy of elastic properties of ultrafine-grained polycrystalline copper after one, two and four passes of equal-channel angular pressing (ECAP) is investigated by means of ultrasonic methods. For each material, Young's and shear moduli in the principal processing directions are evaluated and the symmetry and orientation of the anisotropy are identified. The relation between the determined symmetry and the processing mechanisms is discussed. It is shown that the material after one and two passes of ECAP exhibits a measurable anisotropy, while the material after the fourth pass behaves isotropically. Within the discussion, it is shown that the origin of the observed anisotropy may be attributed to the spatial arrangement of grain boundaries rather than to the crystallographic texture. In the light of this conclusion, the obtained results correspond well with optical and transmission electron microscopy observations of the microstructures of ECAPed materials documented in the literature.

Keywords: Equal-channel angular pressing; Acoustic methods; Copper

1. Introduction

Ultrasonic methods are well-established for the investigation of weak elastic anisotropy induced in polycrystalline metals by manufacturing processes (plastic forming, heat treatment, etc.) [1–3]. For rolled steel sheets, these methods have already been automated for online monitoring during mass production [4,5]. Exact knowledge of the elastic coefficients of rolled sheets is important not only with respect to their further engineering applications; it also enables fast and simple determination of the texture coefficients and, consequently, the plastic strain ratios (e.g. [2]). However, these methods have not yet been applied (except for some preliminary tests done by the current authors in Ref. [6]) to determine the elastic anisotropy of finely grained materials prepared by modern methods of severe plastic deformation (SPD), such as the equal-channel angular pressing (ECAP [7]) or high-pressure torsion (HPT [8]). Unlike rolled sheets, the symmetry of which is relatively high and a priori known (the sheets have orthorhombic anisotropy with the principal axes oriented along the rolling, transverse and normal directions), the symmetry and orientation of the anisotropy of the materials produced by SPD methods are general and unknown, which complicates significantly the use of ultrasonic methods, since in the first step the materials must be always considered as fully triclinic with 21 independent elastic coefficients. A short remark on the elastic anisotropy of ECAPed copper can be found in Ref. [9], where, however, no further details are provided. In later papers concerned with measurements of elastic properties of this material (e.g. [10,11]), the fact

* Corresponding author. Address: Institute of Thermomechanics, Academy of Sciences of the Czech Republic, Dolejškova 5, 18200 Prague, Czech Republic. Tel.: +420 266053712.
E-mail address: hseiner@it.cas.cz (H. Seiner).

1359-6454/$36.00 © 2009 Acta Materialia Inc. Published by Elsevier Ltd. All rights reserved.
doi:10.1016/j.actamat.2009.08.071

that the ECAPed polycrystalline copper could be anisotropic is not taken into account at all. In other words, whereas most other important properties of ECAPed materials, such as crystallographic texture [12], fatigue strength [13] or corrosion resistance [14], have been already thoroughly analyzed, the anisotropy of elasticity remains still uncertain.

In this paper, we apply a combination of two ultrasonic methods, the pulse-echo method and resonant ultrasound spectroscopy (RUS), to determine the evolution of elastic anisotropy of polycrystalline copper during the first few passes of ECAP. It will be shown that although some of the 21 independent elastic coefficients cannot be accurately determined, the output of the applied methods is sufficient for the identification of the classes of symmetry of the examined materials and the evaluation of basic mechanical properties, in particular of Young's and shear moduli in the processing directions. The main aim of this paper is to prove that the ECAPed materials exhibit weak elastic anisotropy, which can be related to the microstructure induced in the material by ECAP processing.

2. Examined material

Technical purity (99.95%) Cu was severely deformed by ECAP to a maximum equivalent strain of $e = 4$ (1, 2, 4 passes) at room temperature following route B_C (specimen rotated by 90° in the same sense about the longitudinal axis after each pass). Prior to ECAP processing the material was annealed for 2 h at 450 °C in a protective inert atmosphere. The billets for ECAP had initial dimensions of 10 mm × 10 mm × 60 mm. The ECAP die used was manufactured from a common tool steel (X38 CrMoV 51). After machining, the die was hardened to 47 HRC. The die had a split design where one part contained the full channel and the other part was used for die closure. The angle Θ between two intersecting channels and the corner angle Ψ were 90° and 0°, respectively. Both channels had a square cross-section of 10 mm × 10 mm. The length of the exit channel was optimized to allow easier processing while maintaining the straight shape of the specimen on exit. The die was placed in a hydraulic Instron 8502 machine which allows a maximum applicable load of 200 kN. Pressing was performed at the speed of 8 mm min^{-1}. Molybdenum disulfide grease was used as a lubricant.

For the ultrasonic measurements, two specimens were cut from each of the examined materials. The individual faces of the prisms were exactly parallel to the X, Y and Z planes of the ECAP billet (the notation of processing planes used here and throughout the whole paper is the same as conventionally used for ECAPed materials [7,15] with the X plane normal to the extrusion direction, the Y plane being the symmetry plane of the channel and the Z plane perpendicular to X and Y planes). To enable a comparison, two similar specimens were also prepared from the original (as-cast) material. The dimensions of the specimens are given in Table 1, where the following notation is used: each specimen is labeled as xPy, where $x = 0, 1, 2, 4$ refers to the number of ECAP passes and $y = 1, 2$ identifies the specimen number. Hereafter in the text, the simpler notation xP will also be used for material after x ECAP passes (without distinguishing between individual specimens). The mass density of all the examined materials was measured by Archimedes's method, giving $\rho = 8.96$ g cm^{-3} for all samples.

Table 1
Dimensions of individual specimens.

Specimen	d_X (mm)	d_Y (mm)	d_Z (mm)
0P1	1.817	3.647	2.700
0P2	1.817	3.644	2.705
1P1	1.812	3.656	2.699
1P2	1.817	3.655	2.695
2P1	1.811	3.650	2.695
2P2	1.816	3.650	2.696
4P1	1.683	3.547	2.710
4P2	1.695	3.546	2.708
Accuracy (mm)	±0.005	±0.005	±0.005

For the purpose of all the measurements described in this paper, all examined materials were considered as homogeneous both in the mass density and in the elastic coefficients. The question of how justified this assumption is falls beyond the scope of this paper. However, the reproducibility of the experimental results presented below (the agreement of results obtained, for example, for specimens 1P1 and 1P2) indicates that the effect of possible heterogeneity on our measurements could be neglected.

3. Experiment

3.1. Ultrasonic methods

The combination of two different experimental methods, namely the pulse-echo method and RUS, was used to analyze the elastic anisotropy of the investigated material. In the following subsections, both methods will be briefly described and their outputs explained and summarized. The reason why these two methods were combined (instead of using only a single one, as is usual) is the following: as was shown recently by the authors [6,16], and will be discussed later in the text, RUS cannot determine all independent elastic coefficients with satisfactory accuracy. In particular, those combinations of elastic coefficients related to longitudinal motion of the material (unidirectional tension/compression, volumetric changes) can be obtained only with high uncertainty. On the other hand, the complete determination of all 21 elastic coefficients by the pulse echo-technique would require measurements in incomparably more directions than the three experimentally achievable on each specimen (directions perpendicular to individual faces). However, the results of pulse-echo measurements in these three directions can provide sufficient information on those coefficients which cannot be determined from RUS output. A similar concept of pulse-echo

Please cite this article in press as: Seiner H et al. Application of ultrasonic methods to determine elastic anisotropy of polycrystalline copper processed by equal-channel angular pressing. Acta Mater (2009), doi:10.1016/j.actamat.2009.08.071

data complementing RUS measurement was previously used successfully on other materials [6,17].

3.1.1. Pulse-echo measurements

The pulse-echo method (e.g. [18]) is the simplest and the most widely used method for the determination of elastic coefficients of solids by ultrasound. This method is based on measurements of times-of-flight of planar ultrasonic pulses between two mutually parallel surfaces of the specimen of the examined material. The same ultrasonic probe is used to generate the pulse and to detect it when it returns reflected from the opposite side of the specimen. The velocity of the wave calculated from the thickness of the specimen in the measurement direction and the time-of-flight contains the information on the elastic properties, as this velocity is fully determined by the mass density and the elastic coefficients. In particular, in any direction **n** of an anisotropic material of density ρ and elastic coefficients C_{ijkl}, the planar waves can propagate only at such (phase) velocities v_φ that [19]

$$\det(C_{ijkl}n_jn_l - \rho v_\varphi^2 \delta_{ik}) = 0, \tag{1}$$

i.e. that ρv_φ^2 is an eigenvalue of the so-called Christoffel matrix $\Gamma_{ik} = C_{ijkl}n_jn_l$. This gives, in general, three different velocities for every direction, each of them corresponding to one mode of propagation. According to the commonly used terminology, the mode with the polarization direction closest to **n** is called quasi-longitudinal (qL) and the other two quasi-transverse (qT). We will use the labels qT1 and qT2 for the faster and the slower modes, respectively.

The pulse-echo method was applied to determine phase velocities of the qL mode in the examined material. These velocities were always measured in directions perpendicular to individual specimen's faces. A 50 MHz pulse/receiver system DPR50+ (JSR Ultrasonics Inc.) and a digital oscilloscope LT264M (LeCroy) were used to generate and to record the pulses. These pulses were sent into the material and detected by a delayed transducer VSP-50 (Ultran Group). The results are listed in Table 2. Whereas for 0P (as-cast material) and for 4P material the velocities in all directions are very similar (the differences are within the range of the experimental errors), in the 1P and 2P material a measurable anisotropy in propagation of the qL mode is observed.

The pulse-echo method was also applied to determine the velocity of transverse waves in the as-cast (0P) material (which was considered as isotropic, i.e. with only one transverse mode of propagation) and of quasi-transverse waves in 1P, 2P and 4P material. In this case, a miniature transducer V157 5/0.125″ (Panametrics) was used. The data are given in Table 3. For most of the anisotropic specimens, the echoes of the two quasi-transverse modes overlapped such that only the velocity of the faster one (qT1) was reliably determinable. Only for directions perpendicular to X and Z of the 2P specimens were the arrivals of the two modes distinguishable.

Table 2
Quasi-longitudinal phase velocities determined in directions perpendicular to individual faces of the individual specimens by pulse-echo measurements. The experimental errors are calculated assuming a 5 μm uncertainty in the specimens' thicknesses and 1 ns in the time-of-flight measurements.

Specimen	v_X^{qL} (mm/μs)	v_X^{qL} (mm/μs)	v_X^{qL} (mm/μs)
0P1	4.735	4.751	4.754
0P2	4.735	4.755	4.758
1P1	4.747	4.770	4.685
1P2	4.741	4.770	4.697
2P1	4.716	4.753	4.665
2P2	4.721	4.751	4.683
4P1	4.752	4.765	4.763
4P2	4.753	4.756	4.766
Accuracy (mm/μs)	±0.018	±0.009	±0.013

Table 3
Transverse and quasi-transverse phase velocities determined in directions perpendicular to individual faces of the individual specimens by pulse-echo measurements. The experimental errors are calculated for the same assumptions as in Table 2. (The higher accuracy in the determination of the transverse wave velocities is given by the fact that the measured times-of-flight are more than two times longer than in the case of qL waves.)

Specimen	v_X^{T} (mm/μs)	v_X^{T} (mm/μs)	v_X^{T} (mm/μs)
0P1	2.331	2.304	2.298
0P2	2.226	2.309	2.299
	v_X^{qT1} (mm/μs)	v_X^{qT1} (mm/μs)	v_X^{qT1} (mm/μs)
1P2	2.190	2.171	2.175
1P1	2.196	2.177	2.172
2P1	2.249	2.205	2.265
2P2	2.256	2.193	2.268
4P1	2.313	2.307	2.310
4P2	2.295	2.306	2.297
	v_X^{qT2} (mm/μs)	v_Y^{qT2} (mm/μs)	v_Z^{qT2} (mm/μs)
2P1	2.156	—	2.191
2P2	2.149	—	2.192
Accuracy (mm/μs)	±0.008	±0.004	±0.005

The velocities of the transverse waves for the 0P material together with the first two rows of Table 2 give, after averaging, the isotropic elastic coefficients of this material:

$$c_{11} = (202.0 \pm 0.6)\text{GPa}, \quad c_{44} = (47.17 \pm 0.5)\text{GPa}. \tag{2}$$

These results are in good agreement with elastic coefficients of commercial (99.85%) polycrystalline copper [20] and will be taken as reference ones. The quasi-transverse velocities obtained for 1P, 2P and 4P materials will be used for independent verification of the results obtained by RUS.

3.1.2. Resonant ultrasound spectroscopy

For the 1P, 2P and 4P specimens, resonant spectra of free elastic vibrations of individual specimens were measured. The method based on measurements and analysis of such spectra is called RUS (e.g. [21]) and belongs among the most advanced and sophisticated ultrasonic techniques for evaluating the elastic properties of anisotropic materials. The relation between the resonant spectra

Please cite this article in press as: Seiner H et al. Application of ultrasonic methods to determine elastic anisotropy of polycrystalline copper processed by equal-channel angular pressing. Acta Mater (2009), doi:10.1016/j.actamat.2009.08.071

and the elastic coefficients of the material is the following: according to Hamilton's principle, the resonant (angular) frequencies ω and the displacement fields of corresponding eigenmodes of vibrations $\mathbf{u}(\mathbf{x})$ of a specimen with known geometry are stationary points of the time-averaged Lagrangian energy:

$$\Lambda(\omega,\mathbf{u}(\mathbf{x}))=\frac{1}{2}\int_V\left[\omega^2\rho u_i u_i-C_{ijkl}\frac{\partial u_i}{\partial x_j}\frac{\partial u_k}{\partial x_l}\right]\mathrm{d}V, \tag{3}$$

where C_{ijkl} and ρ are the tensor of elastic coefficients and mass density of the material, respectively, and V is the specimen volume. The points (i.e. the eigennumbers ω^2 and eigenvectors $\mathbf{u}(\mathbf{x})$) where the variational condition

$$\delta\Lambda(\omega,\mathbf{u}(\mathbf{x}))=0 \tag{4}$$

is satisfied must be found numerically, for which the Ritz method is usually adopted. Consequently, the elastic coefficients must be obtained by an inverse procedure, i.e. by a numerical search for such elastic coefficients that the resonant frequencies corresponding to them fit the experimentally obtained resonant spectra in some optimal way.

The resonant spectra used for the determination of elastic coefficients of the ECAPed copper in this paper were measured by a fully non-contact experimental setup [22]. In this setup, the specimen is excited by an impact of a focused laser pulse (a so-called thermoacoustic source) and the vibrations are detected by laser-Doppler interferometry of the surface of the excited specimen. In this way, not only the resonant frequencies but also the shapes of the eigenmodes are obtained (an enhancement of RUS measurements introduced originally by Ogi et al. [23]). The specimen itself is placed on an underlay which must be extremely acoustically soft (i.e. its acoustic impedance must be insignificant compared to the impedance of the specimen) to ensure a good approximation of the free-surface boundary conditions as required by the variational condition (4).

The vibrations in the examined specimens were excited by sequences of pulses of a focused infrared laser beam (pulse duration 8 ns, energy 25 mJ, Quantel ULTRA Nd:YAG laser system, equipped with fiber optic FOLA options) and the displacement response was detected by a Polytec Micro System Analyzer MSA-500 (using an OFV-5000 controller and an OFV-551 sensor head) for a mesh of 25×25 points evenly covering one face of the specimen. The spectra of specimens $1\mathrm{P}1,\ldots,4\mathrm{P}2$ were measured in the frequency range 150 kHz $\div$ 2 MHz. At least 50 peaks were reliably located for each specimen. For each of the located peaks, a shape of the corresponding mode of vibration was constructed from the amplitudes of this peak in spectra obtained from individual points of the mesh.

For the sake of completeness, let us mention here that the resonant spectra were also measured for the as-cast material (specimens 0P1 and 0P2). The identified peaks in these spectra (20 peaks for each specimen) agreed accurately with resonant frequencies evaluated for coefficients given in Eq. (2).

3.2. Inverse procedure and estimation of experimental errors

From the combined data of the pulse-echo and the RUS measurements, the elastic coefficients for 1P, 2P and 4P material were sought by minimizing a constrained error function (superscripts calc. and exp. denote the calculated and the experimentally obtained quantities):

$$\begin{aligned}F(c_{ij},\lambda_X,\lambda_Y,\lambda_Z)=&\sum_{k=1}^{p}\left(\omega_k^{\mathrm{exp.}}-\omega_k^{\mathrm{calc.}}(c_{ij})\right)^2\\&+\lambda_X\left(v_X^{\mathrm{qL,\,exp.}}-v_X^{\mathrm{qL,\,calc.}}(c_{ij})\right)\\&+\lambda_Y\left(v_Y^{\mathrm{qL,\,exp.}}-v_Y^{\mathrm{qL,\,calc.}}(c_{ij})\right)\\&+\lambda_Z\left(v_Z^{\mathrm{qL,\,exp.}}-v_Z^{\mathrm{qL,\,calc.}}(c_{ij})\right),\end{aligned} \tag{5}$$

where the ω_k are the resonant angular frequencies, c_{ij} are the sought elastic coefficients, $v_X^{\mathrm{qL}}, v_Y^{\mathrm{qL}}$ and v_Z^{qL} are the quasi-longitudinal phase velocities in directions perpendicular to the respective faces (from Table 2), and λ_X,λ_Y and λ_Z are the Lagrange multipliers representing the constrains. The association of the calculated resonant frequencies with the experimental data in the first summation of Eq. (5) was done based on the shapes of the individual modes of vibration as recorded by laser-Doppler interferometry. Only those calculated resonances were taken into account for which their experimental counterparts were reliably identifiable in the spectrum. As initial guesses for the numerical minimization (using a non-linear Levenberg–Marquardt method), isotropic elastic coefficients (2) of the 0P material were taken. For each of the analyzed specimens, a minimum of the function (5) was found such that the misfit between the experimental and computed frequencies did not exceed 0.2% for any of the identified modes.

As for any inverse problem, it is necessary to discuss how accurate the results obtained by minimization of Eq. (5) are. In its unconstrained form, the nature of the RUS measurements directly provides well-justified estimates of the experimental errors with which the individual elastic coefficients are obtained. This method of estimation of the experimental accuracy of the RUS measurements is thoroughly described in Ref. [24] and discussed in Ref. [6,16]; here, only the main findings are summarized: taking $\omega_{1,\ldots,p}$ as the experimentally obtained resonant frequencies and $C_{1,\ldots,K}$ as the unknown elastic coefficients (i.e. $K=3$ for cubic symmetry, $K=9$ for orthorhombic symmetry, etc.), and for partial derivatives $\partial\omega_k/\partial C_l$ obtained numerically within the solution of the variational problem (4), the so-called sensitivity matrix $\mathbf{S}=\mathbf{G}^{\mathrm{T}}\mathbf{G}$ can be constructed, where $G_{ij}=\partial\omega_i/\partial C_j$. In Ref. [24], two important properties of this sensitivity matrix are shown:

1. The sensitivity matrix is symmetric and positive definite, which means that all its eigennumbers $(\lambda_l, l=1,\ldots,K)$ are real and positive and the eigenvectors $(\beta_{kl}, k=1,\ldots,K$ for each $l)$ can be chosen orthonormal.

Please cite this article in press as: Seiner H et al. Application of ultrasonic methods to determine elastic anisotropy of polycrystalline copper processed by equal-channel angular pressing. Acta Mater (2009), doi:10.1016/j.actamat.2009.08.071

2. If the eigenvectors β_{kl} are now known, and C_l^* are linear combinations of the original elastic coefficients $C_{1,\dots,K}$ such that $C_k = \beta_{kl} C_l^*$, we can estimate the experimental error of each combination C_l^* as:

$$\Delta C_l^* = \sqrt{\frac{\sum_{k=1}^{p} (\omega_k^{\text{calc.}} - \omega_k^{\text{exp.}})^2}{\lambda_l}}, \tag{6}$$

where the superscripts calc. and exp. are used to identify the calculated and the experimentally obtained frequencies.

In other words, it is always possible to obtain a set of K orthonormal combinations of the sought elastic coefficients sorted by accuracy with which these combinations may be determined from the particular RUS measurement. The linear relation $C_k = \beta_{kl} C_l^*$ then enables the accuracies ΔC_k to be directly recalculated from ΔC_l^*. In Refs. [6,16,24], it is shown that the combinations with the lowest accuracy (largest experimental error) are often related to the longitudinal motion of the material, and consequently, it is natural to use the qL velocity data from the pulse-echo measurements to stabilize the RUS measurement.

The estimation of the experimental error of the elastic coefficients obtained by constrained optimization (5) can be done using a similar manner, but taking the constraints into account. We assume that close to the optimized elastic coefficients, the constraints $v_{X,Y,Z}^{\text{qL, calc.}}(C_k) = v_{X,Y,Z}^{\text{qL, exp.}}$ can be linearized, i.e. such coefficients $B_{X,Y,Z}^k$ and $B_{X,Y,Z}^0$ can be found that

$$v_X^{\text{qL, calc.}}(C_k) \approx \sum_{k=1}^{K} B_X^k C_k + B_X^0, \tag{7}$$

etc. Such a linearization enables us to write a system of linear equations (utilizing the orthogonality of β_{ij}):

$$\begin{pmatrix} \beta_{11} & \dots & \beta_{K1} \\ \vdots & \ddots & \vdots \\ \beta_{1K} & \dots & \beta_{KK} \\ B_X^1 & \dots & B_X^K \\ B_Y^1 & \dots & B_Y^K \\ B_Z^1 & \dots & B_Z^K \end{pmatrix} \begin{pmatrix} C_1 \\ \vdots \\ C_K \end{pmatrix} = \begin{pmatrix} C_1^* \\ \vdots \\ C_K^* \\ v_X^{\text{qL, exp.}} - B_X^0 \\ v_Y^{\text{qL, exp.}} - B_Y^0 \\ v_Z^{\text{qL, exp}} - B_Z^0 \end{pmatrix} \tag{8}$$

where the experimental accuracy of the right-hand side is known (ΔC_l^* are evaluated in Ref. (6) for the elastic coefficients minimizing the constrained problem (5), and $\Delta v_{X,Y,Z}^{\text{qL, exp.}}$ are taken from Table 2). By dividing each row of this system by the corresponding experimental error, we obtain a similar system but with all the accuracies of the right-hand side equal to 1. As this system is obviously overdetermined, the inverse linear relations can be found in the least-squares sense only. This can be easily done using the Moorse–Penrose pseudoinversion (the authors used the `pinv` routine of the Matlab environment). Thanks to the unit accuracy of the right-hand side, the accuracies of individual elastic coefficients ΔC_k are then directly equal to Euclidean norms of the respective rows of the pseudoinverse matrix.

This approach was used for evaluation of experimental errors of all the elastic coefficients reported in the next section. For each specimen, it was checked that the involvement of the pulse-echo data actually lowered the experimental errors (in particular, that the accuracies of the $c_{11}, c_{22}, c_{33}, c_{12}, c_{13}$ and c_{23} coefficients were significantly improved). Moreover, the correctness of this sensitivity analysis for the constrained inverse problem was verified by a Monte Carlo simulation: for each specimen, the sensitivity matrix $\mathbf{S}$ was constructed and the combinations C_l^* with accuracies ΔC_l^* given by relation (6) were evaluated. Then, a population of 10^6 random sets of these combinations (distributed normally with dispersions $\pm\Delta C_l^*$) was generated. From this population, a subpopulation was selected by taking only these sets for which the evaluated qL velocities $v_{X,Y,Z}^{\text{qL,calc.}}(C_l^*)$ fitted the experimental values $v_{X,Y,Z}^{\text{qL, exp.}}$ with accuracy better than given in Table 2. Using this procedure, subpopulations referred to hereafter as $\mathscr{SP}(1P1), \mathscr{SP}(1P2), \dots, \mathscr{SP}(4P2)$ were obtained, each containing typically 200–300 sets of combinations. The experimental errors obtained by the Monte Carlo simulations and by the pseudoinversion of matrix (8) did not differ by more than 10%.

4. Optimized elastic coefficients

For each specimen, the elastic coefficients were obtained in the form of a full triclinic matrix c_{ij}. In the following section, these matrices will be used for determination of more easily interpretable characteristics of the material, such as the Young's moduli in chosen directions or classes of material symmetry (a complete overview of matrices c_{ij} is given in Section 4.2). The consistency of the obtained results can be easily checked by comparison of velocities of quasi-transverse modes evaluated for them and those determined by the pulse-echo method (Table 3). Such comparison is done in Table 4, which confirms that the evaluated and experimentally obtained values are in good (better than $\pm 2\%$) agreement.

4.1. Summary of mechanical properties

The optimized elastic coefficients were used for the evaluation of elastic moduli in the directions and planes related to the ECAP processing. These are the Young's moduli in directions normal to the planes X, Y and Z (denoted $E_{\perp X}$, $E_{\perp Y}$ and $E_{\perp Z}$) and the shear moduli in these planes (G_X, G_Y and G_Z).

The Young's modulus in a given direction is defined as a coefficient of the linear relation between the magnitude of unidirectional tension applied in this direction and the relative elongation of the material in this direction (i.e. the Young's modulus in the direction x_i satisfies the relation $\sigma_{ii} = E\varepsilon_{ii}$ for all other σ_{jk} equal to zero). Similarly, the shear modulus in a given plane is defined as a coefficient of linear

Please cite this article in press as: Seiner H et al. Application of ultrasonic methods to determine elastic anisotropy of polycrystalline copper processed by equal-channel angular pressing. Acta Mater (2009), doi:10.1016/j.actamat.2009.08.071

relation between a magnitude of pure shear loading applied in this plane and the shear strain in this plane (i.e. the shear modulus in plane $x_i x_j$ satisfies the relation $\sigma_{ij} = 2G\varepsilon_{ij}$ for all other σ_{kl} equal to zero). For a Cartesian coordinate system oriented such that $x_1 \perp X$, $x_2 \perp Y$ and $x_3 \perp Z$, it can be easily shown that $E_{\perp X} = 1/s_{11}$, $E_{\perp Y} = 1/s_{22}$, $E_{\perp Z} = 1/s_{33}$, $G_X = 1/s_{44}$, $G_Y = 1/s_{55}$ and $G_Z = 1/s_{66}$, where s_{ij} is an inverse matrix to c_{ij} (so-called compliance matrix).

In Table 5, the Young's and shear moduli for all specimens are compared. Moreover, for each specimen the bulk modulus K is also provided, which is a coefficient of linear relation between a hydrostatic compression applied on the material and the resultant volumetric change (i.e. the bulk modulus for $\sigma_{11} = \sigma_{22} = \sigma_{33} = \sigma$ satisfies the relation $\sigma = K\mathrm{tr}(\varepsilon)$). The Young's and shear moduli are also plotted in Fig. 1, which depicts both a comparison of individual specimens for 1P, 2P and 4P and a comparison of evolution of individual moduli. It shows (among other things) that the first ECAP pass induces a significant shear softening in all processing planes, which completely disappears after the fourth pass of ECAP. The slight softening in the $E_{\perp X}$ modulus due to the first pass of ECAP was also documented in Ref. [10].

Two general conclusions can be drawn based on Table 5. Firstly, the determination of all moduli is fully reproducible, since the differences between results for specimens 1P1 and 1P2 (as well as for 2P1 and 2P2, and for 4P1 and 4P2) are within the respective experimental errors. Secondly, while all Young's and shear moduli significantly change with each ECAP pass, the bulk modulus is approximately the same for all specimens. This is not surprising, as the observed anisotropy is induced purely by changes in texture and microstructure, while the material (fully dense polycrystalline copper) remains the same. Note here that for single-crystal copper ($c_{11} = 168.4$ GPa, $c_{12} = 121.4$ GPa and $c_{44} = 75.4$ GPa [25]), the value of K is 137.1 GPa, which agrees with the well-known equivalence between the bulk moduli of single crystals and polycrystals (e.g. [26]).

The evolution of the Young's and shear moduli in Table 5 (and Fig. 1) also supports the conjecture already indicated in Table 2 that whereas the 1P and 2P specimens are measurably anisotropic, the material after the fourth pass of ECAP seems to behave isotropically.

4.2. Analysis of particular material symmetries

Knowing now that the anisotropy induced by ECAP pressing is measurable and that our measurements are reproducible (different specimens of the same material give comparable results) and consistent with the origin of the anisotropy (the bulk modulus does not change), we can proceed to the analysis of the symmetry of this anisotropy. In the following subsection, this will be done for 1P, 2P and 4P specimens.

For all examined materials, the symmetry is sought by identification of planes of mirror symmetry of the so-called normal surfaces [19], which are the surfaces of phase velocity magnitudes for the direction of propagation running through a unit sphere. For each material, the normal surfaces of all modes of propagation (one qL mode and two qT modes) are taken into account. We utilize the fact that the anisotropy of the material is fully described by these three surfaces and that these surfaces have the same symmetry elements as the elasticity of the material. The mirror planes are sought using the following procedure:

1. For the experimentally obtained elastic coefficients, the phase velocities of all three modes are evaluated in 400 directions covering a half of a unit sphere.
2. For $\psi \in \langle 0, \pi\rangle$ and $\theta \in \langle 0, \pi\rangle$ (a half-sphere) a function

$$M(\psi,\theta) = \sum_{k=1}^{400}\left(v_k^{\mathrm{qL}}(c_{ij}) - v_k^{\mathrm{qL}}\left(c_{ij}^{M}(\psi,\theta)\right)\right)^2 + \sum_{k=1}^{400}\left(v_k^{\mathrm{qT1}}(c_{ij}) - v_k^{\mathrm{qT1}}\left(c_{ij}^{M}(\psi,\theta)\right)\right)^2 + \sum_{k=1}^{400}\left(v_k^{\mathrm{qT2}}(c_{ij}) - v_k^{\mathrm{qT2}}\left(c_{ij}^{M}(\psi,\theta)\right)\right)^2, \quad (9)$$

is evaluated, where $c_{ij}^{M}(\psi,\theta)$ is a tensor of monoclinic elastic coefficients with the plane of monoclinic (mirror) symmetry equal to $\mathbf{n} = (\sin\psi\cos\theta;\ \cos\psi;\ \sin\psi\sin\theta)$. This tensor is obtained by rotating the original tensor into a coordinate system in which the x_1x_2 plane becomes identical to $\mathbf{n}$, setting the proper elastic coefficients ($c_{14}, c_{24}, c_{34}, c_{15}, c_{25}, c_{35}, c_{46}$ and c_{56}) equal to

Table 4
Quasi-transverse phase velocities evaluated in directions perpendicular to individual faces of the individual specimens from the optimized elastic coefficients. For each velocity, its difference from the corresponding experimentally obtained value (Table 3) is given by $\delta^{\mathrm{mode}}_{\mathrm{direction}}$.

Specimen	v_X^{qT1} (mm/μs)	δ_X^{qT1} (%)	v_Y^{qT1} (mm/μs)	δ_Y^{qT1} (%)	v_Z^{qT1} (mm/μs)	δ_Z^{qT1} (%)
1P1	2.189	−0.26	2.199	−1.01	2.195	−1.07
1P2	2.191	−0.32	2.202	−1.10	2.192	−0.94
2P1	2.249	0.03	2.199	0.27	2.251	0.60
2P2	2.256	−0.01	2.191	0.03	2.261	0.30
4P1	2.317	−0.19	2.312	−0.19	2.329	−0.82
4P2	2.316	−0.90	2.323	−0.76	2.325	−1.24
	v_X^{qT2} (mm/μs)	δ_X^{qT2} (%)	v_Y^{qT2} (mm/μs)	δ_Y^{qT2} (%)	v_Z^{qT2} (mm/μs)	δ_Z^{qT2} (%)
2P1	2.153	0.13	–	–	2.189	0.08
2P2	2.150	−0.08	–	–	2.177	0.69

Please cite this article in press as: Seiner H et al. Application of ultrasonic methods to determine elastic anisotropy of polycrystalline copper processed by equal-channel angular pressing. Acta Mater (2009), doi:10.1016/j.actamat.2009.08.071

zero, and rotating this "monoclinized" tensor back to the original coordinate system.
3. Significant peaks on the surface $1/M(\psi,\theta)$ are sought. Each such peak corresponds to a plane of approximate mirror symmetry.

In order to visualize the anisotropy, the difference between the normal surfaces of qT modes $\Delta v^{\mathrm{qT}}(\mathbf{n}) = v^{\mathrm{qT1}}(\mathbf{n}) - v^{\mathrm{qT2}}(\mathbf{n})$ is used. This difference is identically equal to zero for isotropic materials. For anisotropic materials, symmetry of $\Delta v^{\mathrm{qT}}(\mathbf{n})$ follows, again, the symmetry of the material, having either zeros or local extremes in the principal directions. Note that the anisotropy induced by ECAP passes is weak, and thus plotting the normal surfaces of individual modes themselves (or, for example, surfaces of Young's or shear moduli) would be meaningless, as these surfaces cannot be visually distinguished from spheres.

4.2.1. Material after the first pass of ECAP

In the coordinate system given by the edges of the specimens ($x_1 \perp X, x_2 \perp Y$ and $x_3 \perp Z$), the resulting elastic coefficients for the specimens of the 1P material are:

$$c_{ij}^{\mathrm{1P1}} = \begin{pmatrix} 201.8 \pm 0.5 & 103.7 \pm 0.6 & 111.8 \pm 0.6 & -0.4 \pm 6.3 & 3.1 \pm 3.8 & 1.1 \pm 5.2 \\ & 203.7 \pm 0.3 & 109.8 \pm 0.3 & 0.6 \pm 5.4 & -1.5 \pm 4.2 & 2.5 \pm 4.7 \\ & & 196.6 \pm 0.5 & -0.1 \pm 7.1 & 3.5 \pm 3.6 & 0.0 \pm 5.1 \\ & & & 42.1 \pm 0.1 & 0.5 \pm 0.9 & -1.0 \pm 0.6 \\ & & & & 42.9 \pm 0.3 & -0.1 \pm 0.5 \\ & & & & & 42.4 \pm 0.2 \end{pmatrix} \mathrm{GPa} \tag{10}$$

and

$$c_{ij}^{\mathrm{1P2}} = \begin{pmatrix} 201.3 \pm 0.5 & 104.2 \pm 0.7 & 111.9 \pm 0.5 & 2.0 \pm 5.0 & 0.2 \pm 2.6 & 2.7 \pm 4.0 \\ & 203.8 \pm 0.4 & 109.9 \pm 0.4 & 2.6 \pm 5.1 & -2.6 \pm 2.8 & 1.4 \pm 4.6 \\ & & 197.6 \pm 0.5 & 1.6 \pm 6.4 & 1.9 \pm 2.8 & 1.5 \pm 5.3 \\ & & & 42.1 \pm 0.2 & 0.3 \pm 0.5 & -1.1 \pm 0.6 \\ & & & & 42.9 \pm 0.3 & -0.2 \pm 0.5 \\ & & & & & 42.3 \pm 0.1 \end{pmatrix} \mathrm{GPa}. \tag{11}$$

Here, all elastic coefficients are written in the form $c_{ij} \pm \Delta c_{ij}$, where the mean values c_{ij} are those minimizing the constrained error function (5) and the variations Δc_{ij} were evaluated by pseudoinversion of system (8).

An enormous difference in Δc_{ij} between the diagonal quadrants (upper left quadrant containing coefficients $c_{11}, c_{22}, c_{33}, c_{12}, c_{13}$ and c_{23}; lower right quadrant containing coefficients $c_{44}, c_{55}, c_{66}, c_{45}, c_{46}$ and c_{56}) and the off-diagonal quadrant for both matrices is clearly seen. While the coefficients in diagonal quadrants of c_{ij}^{1P1} and c_{ij}^{1P2} are very similar and are determined with satisfying accuracy (less than ±1 GPa), the coefficients in the off-diagonal quadrant are poorly determined and differ significantly between 1P1 and 1P2. Surprisingly, the constrained optimization (5) cannot provide exact values of the off-diagonal quadrants. However, this precludes neither reliable and accurate evaluation of the Young's and shear moduli (as obvious from Table 5), nor identification of the material symmetry. Indeed, when searching for the planes of the mirror symmetry, the surfaces $M^{-1}(\psi,\theta)$ look like those in Fig. 2, with three significant peaks (denoted A, B and C) for both specimens. If the surface $M^{-1}(\psi,\theta)$ is constructed for all the members of statistical subpopulations $\mathscr{SP}$(1P1) and $\mathscr{SP}$(1P2) (introduced in Section 3.2) and the locations of these peaks are found, we obtain the values listed in Table 6 (considering, again, that the angles ψ and θ are normally distributed). We can conclude that the information obtained from the measurements in the form of matrices c_{ij}^{1P1} and c_{ij}^{1P2} and corresponding subpopulations $\mathscr{SP}$(1P1) and $\mathscr{SP}$(1P2) is sufficient for reliable determination of the symmetry of the examined material, regardless of

Table 5
Young's and shear moduli in the processing directions.

Specimen	$E_{\perp X}$ (GPa)	$E_{\perp Y}$ (GPa)	$E_{\perp Z}$ (GPa)	G_X (GPa)	G_Y (GPa)	G_Z (GPa)	K (GPa)
0P12	127.1 ± 0.6	···	···	47.2 ± 0.5	···	···	139.1 ± 1.5
1P1	126.2 ± 0.5	129.6 ± 0.8	116.2 ± 0.4	42.1 ± 0.3	42.7 ± 0.2	42. 3 ± 0.4	139.1 ± 1.8
1P2	125.5 ± 0.5	129.5 ± 0.4	117.2 ± 0.6	42.0 ± 0.2	42.8 ± 0.3	42.2 ± 0.3	139.2 ± 1.1
2P1	122.6 ± 0.2	126.6 ± 0.4	114.0 ± 0.5	42.8 ± 0.1	45.3 ± 0.7	41.4 ± 0.2	138.6 ± 1.9
2P2	122.7 ± 0.6	127.2 ± 0.5	115.6 ± 0.4	42.6 ± 0.2	45.4 ± 0.3	41.4 ± 0.2	139.0 ± 1.4
4P1	128.0 ± 0.2	128.5 ± 0.4	129.2 ± 0.5	47.2 ± 0.5	46.8 ± 0.7	47.8 ± 0.2	139.0 ± 1.4
4P2	128.3 ± 0.9	127.7 ± 0.3	129.5 ± 0.4	47.3 ± 0.7	46.9 ± 0.1	48.0 ± 0.4	139.0 ± 0.9

Please cite this article in press as: Seiner H et al. Application of ultrasonic methods to determine elastic anisotropy of polycrystalline copper processed by equal-channel angular pressing. Acta Mater (2009), doi:10.1016/j.actamat.2009.08.071

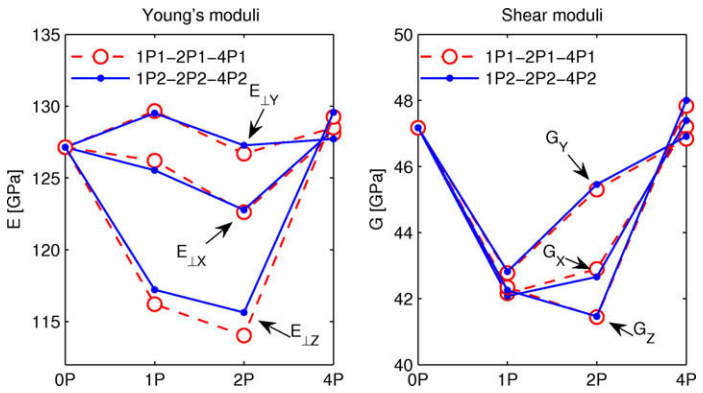

Fig. 1. Evolution of individual elastic moduli with ECAP passes. Agreement between red (dashed, corresponding to specimens 1P1, 2P1 and 4P1) and blue (solid, corresponding to specimens 1P2, 2P2 and 4P2) lines illustrates the reproducibility of the measurements. For 0P, the values of moduli are evaluated from averaged isotropic coefficients (2). (For interpretation of the references to colour in this figure legend, the reader is referred to the web version of this article.)

how large the experimental errors of the off-diagonal quadrants of c_{ij}^{1P1} and c_{ij}^{1P2} are. Note here that the experimental errors of location of the three peaks at the $M^{-1}(\psi,\theta)$ surfaces cannot be determined directly from Δc_{ij}^{1P1} and Δc_{ij}^{1P2}. The reason is that the random variations of individual elastic coefficients are not independent, since the system (8) is overdetermined. The mutual relations between these variations cannot be expressed by Δc_{ij}^{1P1} and Δc_{ij}^{1P2}, but are fully respected by subpopulations $\mathscr{SP}$(1P1) and $\mathscr{SP}$(1P2) from the Monte Carlo simulations.

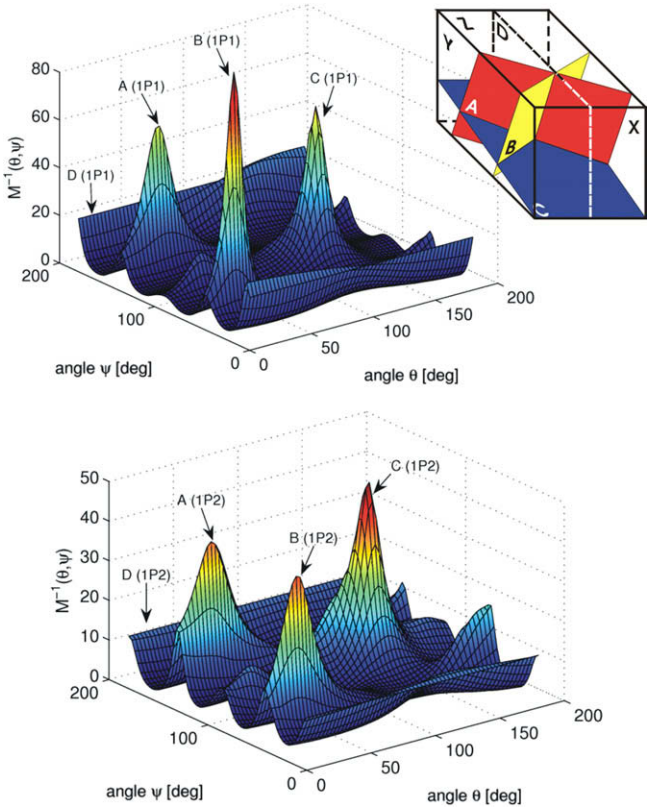

Fig. 2. Surfaces of function $M^{-1}(\psi,\theta)$ for the material after the first pass of ECAP (upper figure corresponds to specimen 1P1, lower figure to 1P2). The peaks A, B and C indicate the planes of significant mirror symmetry. Slightly weaker symmetry can be also found for $\psi = 0°$ (or $\psi = 180°$) as indicated by D. The orientation of individual planes with respect to the processing directions is outlined in the upper right corner.

Let us now return to Fig. 2. The three peaks (A, B and C) shown here correspond to three planes of mirror symmetry, being approximately perpendicular to each other. This indicates that the examined material has an orthorhombic symmetry. The way in which these planes are oriented with respect to the processing direction is also outlined in Fig. 2. The plane C is normal to Y and is declined from Z by approximately 30°; the planes A and B contain an angle of approximately 45° with Y. Such orthorhombic symmetry can be easily related to the microstructure evolution in the material during the first ECAP pass. As observed by Iwahashi et al. [15] in pure aluminum with large grain size and as confirmed by various physical models [27–29], the grains after the first pass of ECAP are elongated in a plane containing an angle of about 30° with the extrusion direction. This corresponds exactly to the plane C identified here from the elastic anisotropy. For our 1P material, the significance of this plane is clearly visible in Fig. 3a, which shows a scanning electron microscopy image of the Y plane with the grain boundaries highlighted by etching. The oriented elongation of the grains was also observed by optical microscopy (Fig. 3b).

Weaker, but still reliably identifiable, symmetry can be found for the Y plane ($\psi = 0°$ or $\psi = 180°$ denoted by D in Fig. 1). This symmetry is due to the symmetry of

Table 6
Locations of planes of approximate mirror symmetry for the 1P specimens. The experimental errors are determined from random subpopulations $\mathscr{SP}$(1P1) and $\mathscr{SP}$(1P2).

Plane label	ψ	θ
A (1P1)	(132.83 ± 1.4)°	(27.3 ± 3.3)°
B (1P1)	(43.13 ± 3.6)°	(25.53 ± 2.4)°
C (1P1)	(92.63 ± 1.7)°	(119.83 ± 0.9)°
A (1P2)	(138.13 ± 2.4)	(31.03 ± 2.6)°
B (1P2)	(48.23 ± 3.4)	(24.53 ± 1.5)°
C (1P2)	(87.73 ± 4.0)	(120.33 ± 1.4)°

Please cite this article in press as: Seiner H et al. Application of ultrasonic methods to determine elastic anisotropy of polycrystalline copper processed by equal-channel angular pressing. Acta Mater (2009), doi:10.1016/j.actamat.2009.08.071

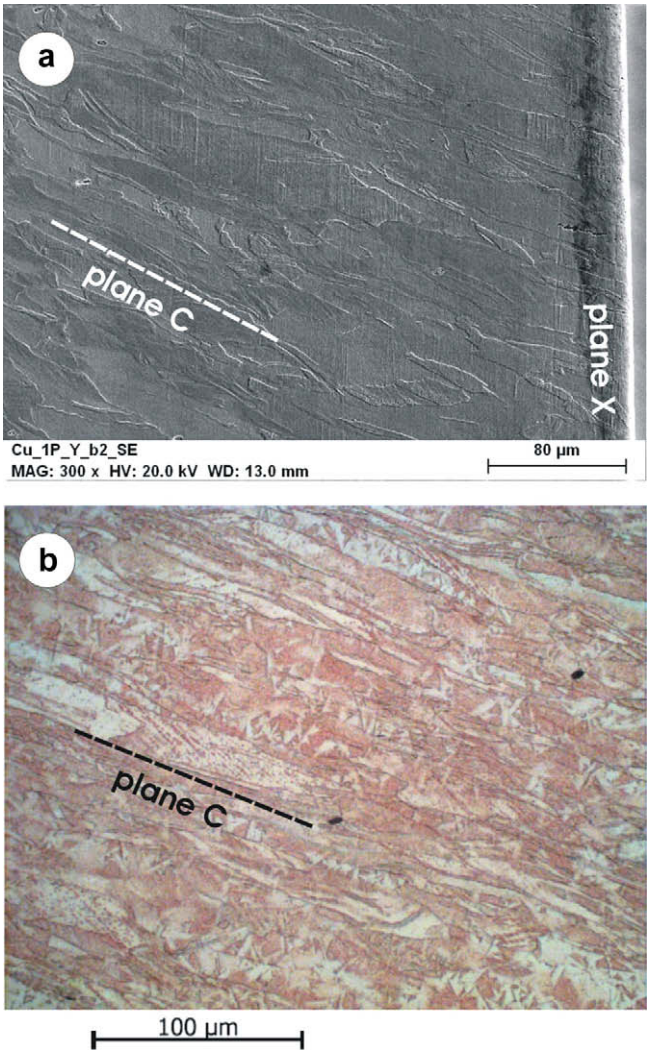

Fig. 3. Grain elongation visible on face *Y*. (a) Scanning electron micrograph with the grain boundaries highlighted by etching (the edge of the specimen (with plane *X*) is visible). (b) Optical micrograph.

processing (the processing die as well as the channel itself are symmetric with respect to this plane). By putting the orthorhombic symmetry given by planes *A*, *B* and *C* and the processing symmetry about plane *Y* together,

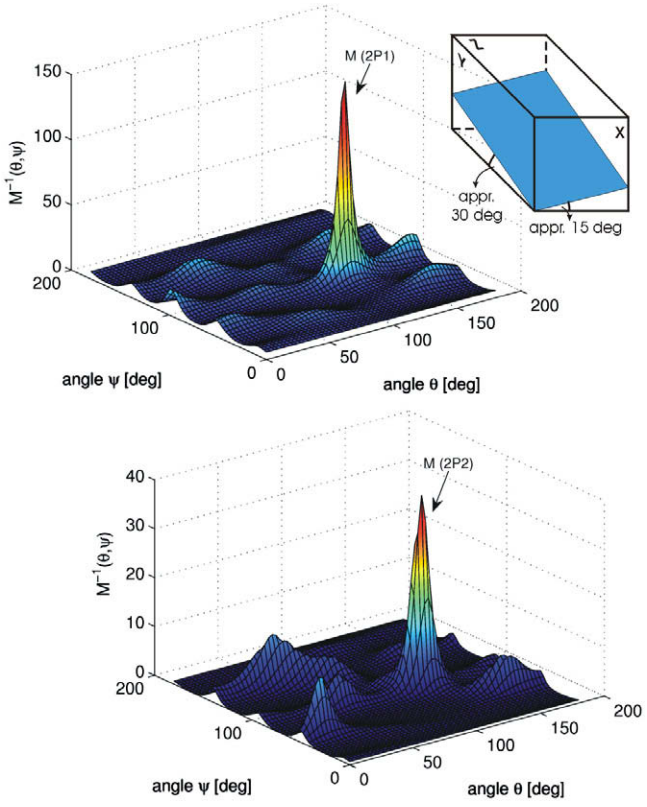

Fig. 5. Surfaces of function $M^{-1}(\psi,\theta)$ for the material after the second pass of ECAP (upper figure corresponds to specimen 2P1, lower figure to 2P2). One significant peak (*M*) indicates the monoclinic symmetry for both specimens. The orientation of the plane *M* with respect to the processing directions is outlined in the upper right corner.

we obtain a tetragonal symmetry with a tetragonal axis normal to plane *C* and with mirror symmetry with respect to planes *A*, *B*, *D* and a plane normal to *C* and *D* (this plane corresponds to the small peak clearly visible between peaks A and B in Fig. 1). If we apply all these symmetry elements to the matrix c_{ij}^{1P} (an average of matrices c_{ij}^{1P1} and c_{ij}^{1P2}), we obtain a tetragonal approximation of the elasticity of the material. In a coordinate system oriented such that x_1 is normal to plane *C* and x_2 and x_3 (which are interchangeable) lie in intersections of

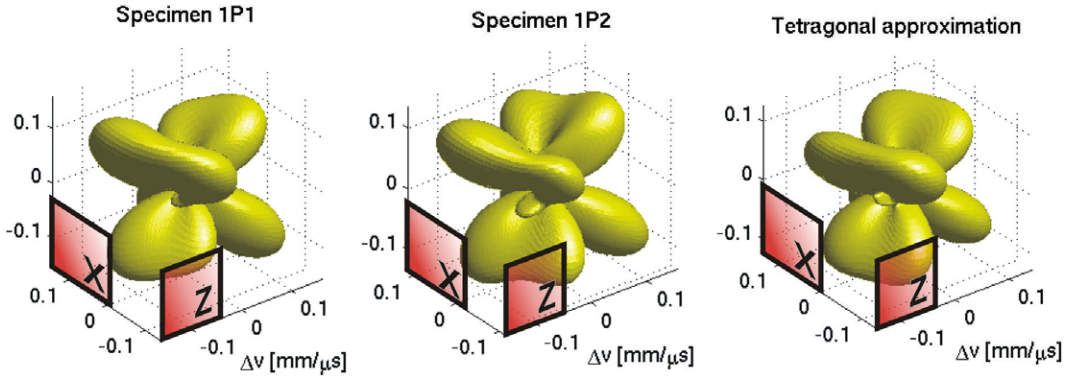

Fig. 4. Comparison of Δv^{qT} surfaces for two specimens of the 1P material and the tetragonal approximation. The orientation of the surfaces with respect to the processing directions is outlined by sketching the *X* and *Z* planes.

Please cite this article in press as: Seiner H et al. Application of ultrasonic methods to determine elastic anisotropy of polycrystalline copper processed by equal-channel angular pressing. Acta Mater (2009), doi:10.1016/j.actamat.2009.08.071

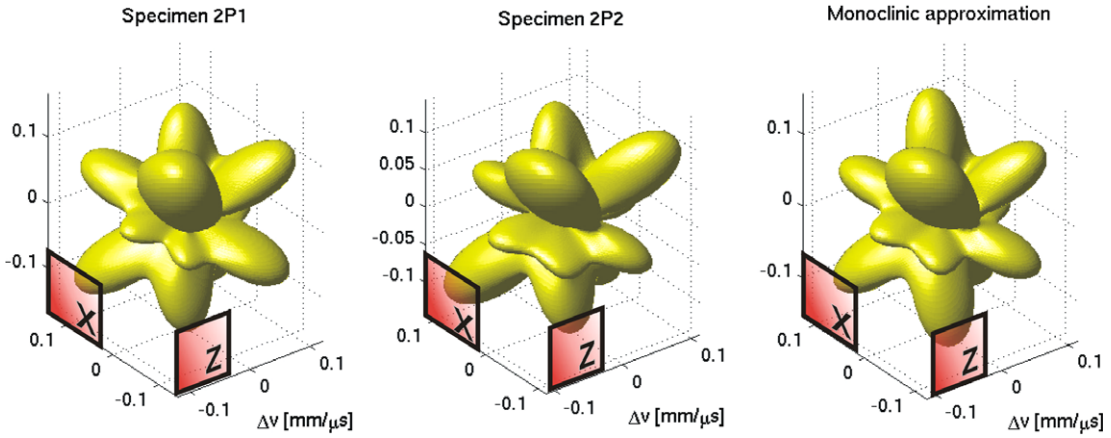

Fig. 6. Comparison of Δv^{qT} surfaces for two specimens of the 2P material and the monoclinic approximation. The orientation of the surfaces with respect to the processing directions is outlined by sketching the X and Z planes.

planes A and B with C, the non-zero elastic coefficients of such approximation are $\tilde{c}_{11}^{1P} = (199.3 \pm 0.7)$ GPa, $\tilde{c}_{22}^{1P} = \tilde{c}_{33}^{1P} = (191.7 \pm 1.2)$ GPa, $\tilde{c}_{44}^{1P} = (50.0 \pm 0.4)$ GPa, $\tilde{c}_{55}^{1P} = \tilde{c}_{66}^{1P} = (43.5 \pm 0.8)$ GPa, $\tilde{c}_{12}^{1P} = \tilde{c}_{13}^{1P} = (112.5 \pm 0.3)$ GPa and $\tilde{c}_{13}^{1P} = (110.3 \pm 0.4)$ GPa. The agreement between the original triclinic results and this approximation is shown in Fig. 4. Moreover, this figure shows again that our measurements are acceptably reproducible, as the agreement between the surfaces of Δv^{qT} for specimens 1P1 and 1P2 is obvious, in spite of the disagreement between the off-diagonal quadrants of matrices c_{ij}^{1P1} and c_{ij}^{1P2}. As the tetragonal approximation also gives a very similar Δv^{qT} surface, we can conclude that the material after one ECAP pass is tetragonal, with a symmetry consistent with the symmetry of ECAP processing and with the tetragonal axis normal to the plane along which the grains are elongated.

4.2.2. Material after the second pass of ECAP

The determined elastic coefficients are:

with the same discrepancy between diagonal and off-diagonal quadrants as for 1P specimens. The procedure for determination of the symmetry planes gives the results shown in Fig. 5. There is only one obvious plane of monoclinic symmetry in this material. This plane has a general orientation $(\theta_{M(2P1)} = (73.5 \pm 3.1)^\circ$, $\psi_{M(2P1)} = (117.1 \pm 2.4)^\circ$, $\theta_{M(2P2)} = (76.1 \pm 2.0)^\circ$ and $\psi_{M(2P2)} = (112.8 \pm 3.9)^\circ$, the experimental errors were determined from subpopulations $\mathscr{SP}(2P1)$ and $\mathscr{SP}(2P2))$ which does not seem to have any relation to any known mechanism of the formation of the microstructure during the second pass. Fig. 6 provides a visual comparison of elastic anisotropy of specimen 2P1, specimen 2P2 and a monoclinic approximation of matrix c_{ij}^{2P} (an average of matrices c_{ij}^{2P1} and c_{ij}^{2P2}). We can conclude that the surfaces of Δv^{qT} are very similar for 2P1 and 2P2 and may be well approximated by the monoclinic symmetry.

4.2.3. Material after the fourth pass of ECAP

The matrices of obtained elastic coefficients for the specimens after the fourth pass of ECAP:

$$c_{ij}^{2P1} = \begin{pmatrix} 199.2 \pm 0.8 & 105.0 \pm 0.1 & 111.7 \pm 1.0 & 1.1 \pm 2.5 & -1.6 \pm 6.0 & 0.6 \pm 5.2 \\ & 202.3 \pm 0.1 & 109.8 \pm 1.3 & -1.7 \pm 2.4 & -2.0 \pm 6.1 & 4.0 \pm 4.4 \\ & & 194.9 \pm 0.4 & 4.5 \pm 2.4 & -0.4 \pm 6.8 & 1.3 \pm 2.4 \\ & & & 43.1 \pm 0.3 & 0.4 \pm 0.3 & 0.5 \pm 2.0 \\ & & & & 45.3 \pm 0.2 & -0.1 \pm 0.7 \\ & & & & & 41.5 \pm 0.1 \end{pmatrix} \text{GPa} \quad (12)$$

and:

$$c_{ij}^{2P2} = \begin{pmatrix} 199.7 \pm 0.5 & 105.1 \pm 0.5 & 112.2 \pm 0.7 & 0.0 \pm 3.4 & 0.7 \pm 6.5 & 0.4 \pm 2.8 \\ & 202.2 \pm 0.1 & 109.6 \pm 0.9 & -1.7 \pm 2.9 & 0.0 \pm 5.9 & 3.3 \pm 3.2 \\ & & 196.4 \pm 0.3 & 3.0 \pm 3.7 & 1.5 \pm 6.5 & 1.9 \pm 4.2 \\ & & & 42.8 \pm 0.5 & 0.9 \pm 0.7 & -0.6 \pm 0.9 \\ & & & & 45.5 \pm 0.2 & -0.6 \pm 0.9 \\ & & & & & 41.5 \pm 0.1 \end{pmatrix} \text{GPa}, \quad (13)$$

Please cite this article in press as: Seiner H et al. Application of ultrasonic methods to determine elastic anisotropy of polycrystalline copper processed by equal-channel angular pressing. Acta Mater (2009), doi:10.1016/j.actamat.2009.08.071

$$c_{ij}^{4P1} = \begin{pmatrix} 202.4 \pm 0.2 & 107.7 \pm 0.5 & 106.6 \pm 0.5 & -0.0 \pm 7.7 & -1.6 \pm 2.5 & -0.9 \pm 5.9 \\ & 202.6 \pm 0.2 & 107.4 \pm 0.8 & 1.4 \pm 6.0 & -3.3 \pm 2.1 & -0.0 \pm 6.0 \\ & & 203.5 \pm 0.3 & 1.8 \pm 5.9 & -1.4 \pm 1.7 & -1.2 \pm 5.3 \\ & & & 47.4 \pm 0.5 & 1.1 \pm 1.0 & -0.5 \pm 1.1 \\ & & & & 47.0 \pm 0.1 & -0.2 \pm 1.0 \\ & & & & & 48.0 \pm 0.2 \end{pmatrix} \text{GPa} \tag{14}$$

and:

$$c_{ij}^{4P2} = \begin{pmatrix} 202.2 \pm 0.4 & 107.7 \pm 0.3 & 106.7 \pm 0.3 & 0.7 \pm 0.9 & -3.1 \pm 5.3 & -2.1 \pm 3.0 \\ & 203.4 \pm 0.2 & 107.5 \pm 0.6 & 0.1 \pm 0.9 & -3.4 \pm 6.0 & -0.6 \pm 2.7 \\ & & 203.2 \pm 0.2 & -0.5 \pm 1.7 & -1.0 \pm 6.1 & -1.7 \pm 2.7 \\ & & & 47.2 \pm 0.1 & 1.4 \pm 0.6 & -0.0 \pm 0.2 \\ & & & & 46.9 \pm 0.2 & -0.5 \pm 0.9 \\ & & & & & 47.8 \pm 0.1 \end{pmatrix} \text{GPa} \tag{15}$$

look similar to the matrices for the 1P and 2P specimens. However, for this material, the differences between, for example, c_{11}, c_{22} and c_{33} are comparable with the experimental errors. This means that it is questionable whether our measurements can reliably identify the elastic anisotropy of this material. Moreover, our algorithm for identification of the mirror planes fails: the $M^{-1}(\psi,\theta)$ surfaces do not contain any significant peaks (but the whole surfaces are slightly shifted upwards), which also supports our conjecture that the 4P material can be sufficiently described by isotropic elasticity. This finding can be quantitatively illustrated by evaluation of anisotropy factors A of individual materials. This factor can be (for general triclinic anisotropy) defined, for example, as $A = \left(v_{\max}^{qT}/v_{\min}^{qT}\right)^2$, where $v_{\max}^{qT}$ and $v_{\min}^{qT}$ are the maximal and the minimal quasi-transverse velocity, respectively. For a cubic single crystal of copper, this definition is equivalent to the classical definition for cubic materials $A = 2c_{44}/(c_{11} - c_{12})$, and gives $A = 3.21$. For the 1P, 2P and 4P materials (always taking the average values of c_{ij} for the two examined specimens), the respective coefficients are as follows: $A^{1P} = 1.23$, $A^{2P} = 1.21$ and $A^{4P} = 1.08$. This, again, confirms that the anisotropy of the 4P material is significantly smaller than that of 1P or 2P (which are comparable to each other). By minimizing an error function similar to (9), we can find the isotropic constants giving the best approximation of the 4P material. These values ($c_{11} = 202.7$ GPa and $c_{44} = 47.8$ GPa) are very close to the coefficients of the 0P material (2). In other words, the grain refinement induced by the four ECAP passes (route B_C) does not change the elasticity of the material. This general conclusion is in good agreement with commonly accepted models of shearing processes during the ECAP. It is well known that the material after one and two passes of ECAP contains elongated grains, while almost equiaxed grains are observed in the material after four passes of pressing by route B_C (in Ref. [15], both the theoretical explanation of this effect and an illustrative transmission electron microscopy image can be found).

5. Discussion

As mentioned in the Introduction, measurements of the elastic anisotropy of polycrystalline metals are commonly used for investigation of the texture, i.e. for determination of preferred orientation of the crystallites in a polycrystalline aggregate. It can be shown (e.g. [1]) that for aggregates with orthorhombic or higher symmetry (which is satisfied by the tetragonal symmetry of the 1P material) and for the single crystals with cubic symmetry (which is also valid for copper), the anisotropy given by the texture can be, as a first-order approximation, fully described by three independent crystallite orientation distribution function (CODF) coefficients, usually denoted as W_{400}, W_{420} and W_{440}. In Ref. [2], these coefficients are determined for rolled steel sheets from ultrasonic measurements (using an EMAT technique similar to RUS) and it is shown that the CODF evaluated for these coefficients gives a surprisingly good approximation of the CODF obtained by X-ray measurements. In this section, we will discuss the possibility of similarly estimating the CODF coefficients of the 1P and 2P material from the elastic anisotropy. We will distinguish between the two possible origins of the anisotropy: the crystallographic texture and the microstructure. These two terms will be used in the same sense as in most of the literature concerned with ECAP (e.g. the review papers Refs. [7,12]), which means that the anisotropy induced by the texture will be the anisotropy given by the preferred crystallographic orientation of individual crystallites in the polycrystalline material, whereas the anisotropy induced by the microstructure will be the anisotropy given by the anisotropic spatial arrangement of grain boundaries (typically the grain elongation in 1P and 2P material).

The relation between the elastic coefficients of a textured aggregate c_{ij}, the elastic coefficients of the single crystal C_{ij} and the CODF coefficients can be, in general, written in the form of:

$$c_{ij} = \overline{c}_{ij}(C_{ij}) + c_0(C_{ij}) f(W_{400}, W_{420}, W_{440}), \tag{16}$$

Please cite this article in press as: Seiner H et al. Application of ultrasonic methods to determine elastic anisotropy of polycrystalline copper processed by equal-channel angular pressing. Acta Mater (2009), doi:10.1016/j.actamat.2009.08.071

where the mean (isotropic) elastic coefficients $\overline{c}_{ij}$ and the parameter c_0 depend not only on the single-crystal elastic coefficients C_{ij} but also on the chosen averaging method, whereas f is a function of the CODF coefficients only, independent of the averaging method. Hirao and Ogi [3] give a complete overview of explicit formulas for $\overline{c}_{ij}$ and c_0 for Voigt's method (averaging directly the stiffness matrices C_{ij}), Reuss's method (averaging the compliance matrices $S_{ij} = C_{ij}^{-1}$) and Hill's method, which is a combination of Voight's and Reuss's methods.

It is obvious that the determination of the CODF coefficients $W_{400}W_{420}$ and W_{440} from ultrasonic measurements by inverting the relation (16) is meaningful only under the two following conditions:

1. The mean elastic coefficients $\overline{c}_{ij}$ obtained by the chosen averaging method are good approximations of the elastic coefficients of an untextured aggregate of the examined material, i.e. the difference between the real mean elastic coefficients and the isotropic approximations $\overline{c}_{ij}$ is smaller than the perturbation $c_0(C_{ij})\ f(W_{400}, W_{420}, W_{440})$ attributed to the texture.
2. The anisotropy is fully given by the texture, i.e. the elastic coefficients of a "super-aggregate" (an aggregate of randomly oriented aggregates with elastic coefficients c_{ij}) must be equal to $\overline{c}_{ij}$.

We will show that none of these conditions is fulfilled for our 1P and 2P materials.

In the first three rows of Table 7, the elastic coefficients of a single crystal of copper [25] and of the isotropic polycrystalline aggregates 0P and 4P are listed (the former determined by pulse-echo measurements, the latter by RUS as described in the previous sections). Let us now check which of the available averaging methods gives the best approximation of the polycrystalline aggregates. Ledbetter [30] has provided an analysis showing that neither Voigt's nor Reuss's method, nor their average (Hill's method), is suitable for the evaluation of the elastic coefficients of copper, and that the only method giving acceptable results in this case is the Hershey–Kröner–Eshelby method [31] based on considering an anisotropic inhomogeneity embedded in an isotropic matrix. Indeed, when repeating the calculations after [30], we obtain the results listed in the middle part of Table 7. Only the Hershey–Kröner–Eshelby method gives a reasonably accurate approximations of the constants obtained by pulse-echo and RUS measurements. Unfortunately, no relation for the parameter c_0 from (16) for this method is available in the literature, which makes the formula (16) useless for texture analysis of our 1P and 2P specimens.

Table 7
Comparison of the elastic coefficients of a single crystal of copper (the first row), the coefficients of isotropic polycrystals obtained experimentally on 0P and 4P specimens (the second and the third row), isotropic elastic coefficients evaluated by different averaging methods (middle part of the table) and the isotropic coefficients obtained by averaging of the experimentally obtained coefficients of 1P and 2P specimens.

	c_{11} (GPa)	c_{12} (GPa)	c_{44} (GPa)
Single crystal	168.4	121.4	75.4
0P (pulse-echo)	202.0	107.6	47.2
4P (RUS)	202.7	107.2	47.8
$\overline{c}_{ij}$ (Voigt)	209.9	100.7	54.6
$\overline{c}_{ij}$ (Reuss)	180.7	146.2	17.2
$\overline{c}_{ij}$ (Hill)	195.7	123.4	35.9
$\overline{c}_{ij}$ (Hershey–Kröner–Eshelby)	201.3	104.9	48.2
c^{1P1} (Voigt)	197.7	110.3	43.7
c^{1P2} (Voigt)	197.2	110.3	43.4
c^{1P1} (Reuss)	197.5	110.1	43.7
c^{1P2} (Reuss)	197.1	110.1	43.5
c^{2P1} (Voigt)	197.7	109.6	44.1
c^{2P2} (Voigt)	196.9	109.6	43.7
c^{2P1} (Reuss)	197.7	109.9	43.9
c^{2P2} (Reuss)	197.3	109.9	43.7

A slightly deeper insight in the nature of the elastic anisotropy of the 1P and 2P materials can be obtained by discussing the second condition, i.e. by constructing a super-aggregate. For the experimentally obtained c_{ij} of the 1P and 2P material, this was done numerically by generating 10^6 random orientations (matrices $R_{ij}^{(n=1,\dots,10^6)} \in$ S0(3)) and calculating the Voigt's average:

$$\overline{c}_{ijkl} = \sum_n R_{ia}^{(n)} R_{jb}^{(n)} R_{kc}^{(n)} R_{ld}^{(n)} c_{abcd} \tag{17}$$

and the Reuss's average

$$\overline{c}_{ijkl} = \left(\sum_n R_{ia}^{(n)} R_{jb}^{(n)} R_{kc}^{(n)} R_{ld}^{(n)} c_{abcd}^{-1} \right)^{-1}. \tag{18}$$

Due to the extremely weak anisotropy of the 1P and 2P materials, both averaging methods give approximately the same results, as shown in the lower half of Table 7. (The weakness of the anisotropy also makes the use of both these methods fully justified.) However, the obtained results agree neither with the experimental data for the 0P and 4P materials, nor with the corresponding Hershey–Kröner–Eshelby approximation. In particular, the differences in c_{44} are obvious and cannot be attributed to experimental errors. On the other hand, the bulk modulus remains the same, as can be easily checked ($K = \overline{c}_{11} - \frac{4}{3}\overline{c}_{44}$ for isotropic materials).

We can clearly conclude that the elastic anisotropy of the 1P and 2P materials is not given solely by the texture. It seems that the anisotropy is rather related to the preferred orientation of the grain boundaries (the most apparent evidence for such conclusion is the C plane in the 1P material), which is also consistent with the fact that for the 4P material, where the grains are equiaxed, the elasticity returns to the original isotropic state.

6. Conclusions

We have shown that specimens of polycrystalline copper after the first and the second pass of ECAP exhibit measur-

Please cite this article in press as: Seiner H et al. Application of ultrasonic methods to determine elastic anisotropy of polycrystalline copper processed by equal-channel angular pressing. Acta Mater (2009), doi:10.1016/j.actamat.2009.08.071

able elastic anisotropy, and that the applied ultrasonic methods (a combination of RUS and the pulse-echo method) are suitable for experimental examination of this anisotropy. For the 1P material, the orientation of the experimentally determined tetragonal symmetry can be clearly related to the grain elongation along the plane containing approximately the angle 30° with the Z plane and normal to the Y plane. The 2P material exhibits monoclinic symmetry along a plane which we were unable to relate to any significant plane given by the microstructure. After the fourth pass (4P), the material is isotropic, with elastic coefficients very close to those determined for the material in the initial state (as-cast, 0P).

The bulk modulus of the material does not change during the first four passes of ECAP, while the mean elastic coefficients (isotropic coefficients obtained by averaging methods) are slightly changing. This leads us to the conclusion that the anisotropy we observe for 1P and 2P materials is not given only by the texture, but also by the microstructure, i.e. by the orientation of the grain boundaries, etc.

Acknowledgement

The authors would like to express their thanks to J. Zídek for design and implementation of photoacoustic parts of the experimental setup and for help with manuscript preparation. H.S., L.B., P.S. and M.L. acknowledge supports from the Projects Nos. 101/09/0702 and 202/09/P164 of the Czech Science Foundation, the Project IAA200100627 of the Grant Agency of ASCR, the institutional Project of IT ASCR, v.v.i., CEZ:AV0Z20760514, and from the research center 1M06031 of the Ministry of Education. M.J. and R.K. acknowledge financial support by GAAV under the Grant IAA101120803. O.S. acknowledges financing by GAUK through the Grant No. 8811/2008.

References

[1] Hirao M, Aoki K, Fukuoka H. J Acoust Soc Am 1987;81:1434.
[2] Kawashima K. J Acout Soc Am 1990;87:681.
[3] Hirao M, Ogi H. EMATs for science and industry. Dordrecht: Kluwer; 2003.
[4] Akagi T, Kawashima K, Nawata Y, Hyoguchi T, Yoshiwara A, Hayato K. Nippon Steel Tech Report 1997;74:43.
[5] Moreau A, Levesque D, Lord M, Dubois M, Monchalin JP, Padioleau C, et al. Ultrasonics 2002;40:1047.
[6] Landa M, Seiner H, Sedlák P, Bicanová L, Zídek J, Heller L. Resonant ultrasound spectroscopy close to its applicability limits. In: Everett M, Pedroza S, editors. Horizons in world physics, vol. 246. New York: Nova Publishers; 2009. in press.
[7] Valiev RZ, Langdon TG. Prog Mater Sci 2006;51:881.
[8] Xu C, Horita Z, Langdon TG. Acta Mater 2007;55:203.
[9] Akhmadeev NA, Kobelev NP, Mulyukov RR, Soifer YaM, Valiev ZR. Acta Metall Mater 1993;41:1041.
[10] Lebedev AB, Burenko YuA, Romanov AE, Kopylov VI, Filonenko VP, Gryaznov VG. Mater Sci Eng A 1995;203:165.
[11] Kobelev N, Kolyvanov E, Estrin Y. Acta Mater 2008;56:1473.
[12] Beyerlein IJ, Tóth LS. Prog Mater Sci 2009;54:427.
[13] Vinogradov A, Nagasaki S, Patlan V, Kitagawa K, Kawazoe M. Nanostruct Mater 1999;11:925.
[14] Hadzima B, Janeček M, Hellmig RJ, Kutnyakova Y, Estrin Y. Mater Sci Forum 2006;503–504:883;.
[15] Iwahashi Y, Furukawa M, Horita Z, Nemoto M, Langdon TG. Metall Mater Trans A 1998;29:2245.
[16] Landa M, Sedlák P, Seiner H, Heller L, Bicanová L, Šittner P, et al. Appl Phys A 2009;96:557.
[17] Landa M, Sedlák P, Seiner H, Bicanová L, Šittner P, Novák V. In: Proceedings of international congress on ultrasonics, Vienna, CD-ROM; 9–12 April 2007. <http://www.icultrasonics.org/>.
[18] Papadakis EP, Lerch TP. Pulse superposition, pulse overlap and related techniques. In: Levy M, Bass HE, Stern RR, editors. Handbook of elastic properties of solids, liquids and gases, vol. 1. San Diego, CA: Academic Press; 2001. p. 39.
[19] Auld B. Acoustic fields and waves solids, vol. 1. John Wiley; 1973.
[20] Schneider E. Ultrasonic techniques. In: Hauk V, editor. Structural and residual stress analysis by nondestructive methods. Amsterdam: Elsevier; 1997. p. 522.
[21] Migliori A, Sarrao JL, Visscher WM, Bell TM, Lei M, Fisk Z, et al. Physica B 1993;83:1.
[22] Sedlák P, Landa M, Seiner H, Bicanová L, Heller L. Non-contact resonant ultrasound spectroscopy for elastic constants measurement. In: Abstract, proceedings of the 1st international symposium on laser ultrasonics: science, technology and applications [CD-ROM]. Kirchwald: The e-Journal of Nondestructive Testing; 2008.
[23] Ogi H, Sato K, Asada T, Hirao M. J Acoust Soc Am 2002;112:2553.
[24] Sedlák P. PhD thesis. Czech Tech. Univ. in Prague; 2008.
[25] Musgrave MJP. Crystal acoustics. San Francisco, CA: Holden-Day; 1970.
[26] Chandrasekar S, Santhanam S. J Mat Sci 1989;24:4265.
[27] Kim HS, Estrin Y. Mat Sci Eng A 2005;410–411:285.
[28] Han WZ, Zhang ZF, Wu SD, Li SX. Mat Sci Eng A 2008;476(1–2):224.
[29] Kamachi M, Furukawa M, Horita Z, Langdon TG. Mat Sci Eng A 2003;347(1–2):223.
[30] Ledbetter HM. J Phys D 1980;13:1879.
[31] Eshelby JD. Elastic inclusions and inhomogeneities. In: Sneddon IN, Hill R, editors. Progress in solid mechanics, vol. 2. Amsterdam: North-Holland; 1961. p. 89.

Please cite this article in press as: Seiner H et al. Application of ultrasonic methods to determine elastic anisotropy of polycrystalline copper processed by equal-channel angular pressing. Acta Mater (2009), doi:10.1016/j.actamat.2009.08.071